J|A|C|S ARTICLES

Published on Web 07/10/2009

Anisotropic Fermi Couplings Due to Large Unquenched Orbital Angular Momentum: Q-Band ^{1}H, ^{14}N, and ^{11}B ENDOR of Bis(trispyrazolylborate) Cobalt(II)

William K. Myers,[†] Charles P. Scholes,[‡] and David L. Tierney*,[†]

Department of Chemistry and Chemical Biology, University of New Mexico, Albuquerque, New Mexico 87131, and Department of Chemistry, Center for Biochemistry and Biophysics, University at Albany, SUNY, Albany, New York 12222

Received February 4, 2009; E-mail: dtierney@unm.edu

Abstract: We report Q-band ENDOR of ^{1}H, ^{14}N, and ^{11}B at the $g_{\|}$ extreme of the EPR spectrum of bis(trispyrazolylborate) cobalt(II) [Co(Tp)$_2$] and two structural analogs. This trigonally symmetric, high-spin (hs) $S = 3/2$ Co(II) complex shows large unquenched ground-state orbital angular momentum, which leads to highly anisotropic electronic g-values ($g_{\|} = 8.48$, $g_{\perp} = 1.02$). The large g-anisotropy is shown to result in large dipolar couplings near $g_{\|}$ and uniquely anisotropic ^{14}N Fermi couplings, which arise from spin transferred to the nitrogen 2s orbital (2.2%) via antibonding interactions with singly occupied metal $d_{x^2-y^2}$ and d_{z^2} orbitals. Large, well-resolved ^{1}H and ^{11}B dipolar couplings were also observed. Taken in concert with our previous X-band ENDOR measurements at $g_{\perp}$ (Myers, W. K.; et al. *Inorg. Chem.* **2008**, *47*, 6701−6710), the present data allow a detailed analysis of the dipolar hyperfine tensors of two of the four symmetry distinct protons in the parent molecule. In the substituted analogs, changes in hyperfine coupling due to altered metal−proton distances give further evidence of an anisotropic Fermi contact interaction. For the pyrazolyl 3H proton, the data indicate a 0.2 MHz anisotropic contact interaction and ∼4% transfer of spin away from Co(II). Dipolar coupling also dominates for the axial boron atoms, consistent with their distance from the Co(II) ion, and resolved ^{11}B quadrupolar coupling showed ∼30% electronic inequivalence between the B−H and B−C sp^3 bonds. This is the first comprehensive ENDOR study of any hs Co(II) species and lays the foundation for future development.

Introduction

High spin (hs) $S = 3/2$ Co(II) compounds are of intrinsic physical−inorganic interest because of their large unquenched orbital angular momentum and the magnetic properties that result. In addition, the Co(II) ion is an important spectroscopic surrogate for biological zinc.[1,2] The seminal spin Hamiltonian formalism that Abragam and Pryce applied to tetragonal and trigonal Co(II) chelates in Tutton salt provided a wide-ranging, symmetry-based, crystal-field method for arriving at eigenfunctions, eigenvalues, **g**-tensors, and hyperfine couplings of the Co(II) ion.[3,4] Ligand field methods including the potential for covalent spin transfer were subsequently utilized.[5]

In the 1960s Jesson applied the general spin Hamiltonian theory to bis(trispyrazolylborate) cobalt(II),[6−9] Co(Tp)$_2$, shown in Figure 1.[10−12] The combination of a trigonal distortion and spin−orbit coupling operating on the $^{4}T_{1g}$ octahedral configuration of Co(II) leads to six low-lying Kramers doublets. These eigenstates have large contributions of quartet spin and unquenched orbital angular momentum. The electron spin and orbital angular momentum of the lowest, ground-state eigenfunction account well for the unusual ground-state g-values ($g_{\perp} \approx 1$ and $g_{\|} \approx 8.5$) and for a ground-state ^{59}Co hyperfine tensor having a very large parallel component.[6] Jesson, with subsequent modifications by McGarvey,[13] considered the panoply of all the low-lying doublets in accounting for the NMR hyperfine shifts of the four symmetry distinct sets of protons (Figure 1). The through-space dipolar interaction (often referred to as a pseudo-contact interaction in the context of NMR), which depends on the inverse cube of the metal−proton distance, and the Fermi contact interaction, dependent on the direct transfer of electron spin to the s orbital of a proton, were distinguished via the temperature-dependence of the NMR hyperfine shift. Expressions for the anisotropic modification of the Fermi coupling were developed. These expressions reflect the anisotropic electron spin expectation values ($\langle S_x \rangle$, $\langle S_y \rangle$, and $\langle S_z \rangle$) and afforded the

[†] University of New Mexico.
[‡] University at Albany, SUNY.

(1) Maret, W.; Vallee, B. L. *Methods Enzymol.* **1993**, *226C*, 52–71.
(2) Parkin, G. *Chem. Rev.* **2004**, *104*, 699–767.
(3) Abragam, A.; Pryce, M. H. L. *Proc. R. Acad. Sci. A* **1951**, *205*, 135–153.
(4) Abragam, A.; Pryce, M. H. L. *Proc. R. Acad. Sci. A* **1951**, *206*, 173–190.
(5) Thornley, J. H. M.; Windsor, C. G.; Owen, J. *Proc. R. Soc. (London)* **1965**, *284*, 252–271.
(6) Jesson, J. P. *J. Chem. Phys.* **1966**, *45*, 1049–1056.
(7) Jesson, J. P. *J. Chem. Phys.* **1967**, *47*, 579–581.
(8) Jesson, J. P. *J. Chem. Phys.* **1967**, *47*, 582–591.
(9) Jesson, J. P.; Trofimenko, S.; Eaton, D. R. *J. Am. Chem. Soc.* **1967**, *89*, 3148–3158.
(10) Myers, W. K.; Duesler, E. N.; Tierney, D. L. *Inorg. Chem.* **2008**, *47*, 6701–10.
(11) Trofimenko, S. *J. Am. Chem. Soc.* **1967**, *89*, 3170–3177.
(12) Trofimenko, S., *Scorpionates: The Coordination Chemistry of Polypyrazolylborate Ligands*; Imperial College Press: London, 1999.
(13) McGarvey, B. R. *J. Chem. Phys.* **1970**, *53*, 86–91.

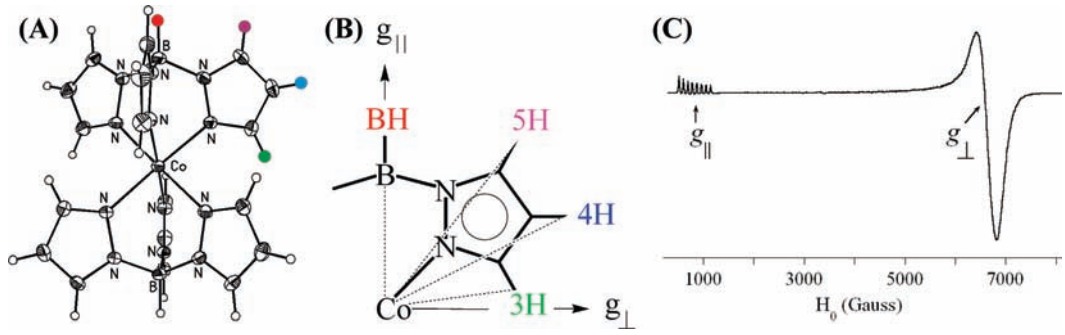

Figure 1. (A) Axial view of bis(trispyrazolylborate) cobalt(II) and the orientation of its magnetic axes. (Reprinted with permission from ref 10. Copyright 2008 American Chemical Society.) The colored spheres in part A represent the symmetry-distinct sets of protons, according to the color scheme in part B, which is followed throughout. The pseudo-octahedral symmetry at the metal provided by the six pyrazolyl nitrogens is reduced by a trigonal distortion along the B···Co···B axial direction (overall symmetry D_{3d}). Two alkyl-substituted analogs were studied to aid in assignment of spectra, uniformly incorporating methyl groups in place of the 3H protons [$Co(Tp^{3Me})_2$] or *n*-butyl groups in place of the BH protons [$Co(n\text{BuTp})_2$]. (C) X-band (9.4 GHz) EPR spectrum of $Co(Tp)_2$, showing $g_{||} = 8.48$ and $g_{\perp} = 1.02$.

first observation of an anisotropic Fermi interaction and a nonzero trace dipolar interaction,[6,13] subsequently identified in other $S = 3/2$ d^7 complexes[14] and complexes of lanthanide ions.[15]

A comprehensive picture of the electronic structure of this magnetically unusual, historically significant complex,[11,12] which forms the basis for more detailed studies of Co(II)-substituted metalloenzymes, requires a thorough experimental elucidation of the ground-state hyperfine couplings to the coordinating ^{14}N, nearby ^{1}H and the unique ^{11}B, without the complexity introduced by population of excited states in fluid solution. However, despite the long-standing historical[4] and biological[1] interest in hs Co(II), ENDOR of hs Co(II) is practically nonexistent. The fast spin−lattice relaxation of the $S = 3/2$ Co(II) ion and the very large field dispersion typical of its EPR spectra have made high-sensitivity ENDOR difficult. To date, only two relevant studies have been reported. The first was an ENDOR study of a DNA-binding Cys_2/His_2 Zn-finger protein, where Zn(II) was replaced by Co(II) at a site of tetrahedral symmetry.[16] The major focus of that short communication was ^{31}P ENDOR due to nearby DNA, which was obtained at only one *g*-value (2.4), although cysteine proton and histidine nitrogen ENDOR were reported at the same *g*-value in the Supporting Information.[16]

The second of these reports was our recent work on the present set of compounds at X-band (~9.4 GHz), which established that the **g**-tensor directions (Figure 1), as indicated in earlier single-crystal EPR studies,[6] are retained in frozen solution.[10] At X-band, ENDOR signals could be obtained at $g_{\perp} \sim 1$, but not near $g_{||} \sim 8.5$. The lack of available data at both the parallel and perpendicular extremes of the EPR spectrum precluded a more detailed analysis, and the data were interpreted in terms of isotropic Fermi contact couplings and traceless dipolar couplings. In the present study, we present Q-band ENDOR from a subset of these compounds, taking advantage of the greater sensitivity at higher frequency to obtain data at $g_{||} \sim 8.5$. Proton assignments were aided by examination of two alkyl-substituted analogs, with analogy to our previous work (see Figure 1).[10] In the course of determining hyperfine parameters and relating them to underlying electronic structure, we note and explain unusually anisotropic magnetic effects brought on by the large spin and orbital angular momentum of the ground state. Combination of our preceding X-band results with those of the present study shows that intrinsically isotropic Fermi couplings are made to appear highly anisotropic and proton dipolar couplings become nontraceless with extremely large values in the parallel direction.

The goal of the present ENDOR study is to provide a more systematic probe of the electronic structure of the ground state of a Co(II) complex. Chosen because of its long-standing interest and complex ground state, $Co(Tp)_2$ has important electronic structural aspects, such as the spin density on the coordinating nitrogens, that have yet to be determined. While $Co(Tp)_2$ has high symmetry and six-coordination, both unexpected in the typical four- or five-coordinate sites encountered in Zn(II) metalloproteins, the Tp ligand has long been used to mimic the trihistidine motif common to biological zinc sites.[1,2,17−19] With only two previous ENDOR studies of frozen solution high-spin Co(II) in the literature,[10,16] much remains for characterizing ligand−Co(II) hyperfine interactions and relating them to the underlying electronic structure of the Co(II) ion.

Materials and Methods

All of the complexes studied here were prepared as described previously.[10] Samples for ENDOR were 5 mM in 1:1 toluene-d_8/CD_2Cl_2; samples for EPR were 20 mM. All samples were thoroughly degassed prior to data collection.

ENDOR Spectroscopy. Q-band (34.1 GHz) ENDOR was performed with a cryogenically tunable TE_{011} resonator[20] at ~2 K.[21−24] ENDOR spectra were recorded by monitoring the radio frequency (rf)-induced change in the rapid-passage, 100 kHz field-modulated EPR signal as the rf was swept. Unless otherwise indicated, the

(14) McGarvey, B. R. In *Foundations of Modern EPR*; Eaton, G. G., Eaton, S. S., Salikhov, K. M., Eds.; World Scientific: Singapore, 1998; *Vol. B*, pp 150−160.
(15) McGarvey, B. R. *J. Chem. Phys.* **1979**, *70*, 4971–4973.
(16) Walsby, C. J.; Krepkiy, D.; Petering, D. H.; Hoffman, B. M. *J. Am. Chem. Soc.* **2003**, *125*, 7502–7503.
(17) Chiou, S.-J.; Riordan, C. G.; Rheingold, A. L. *Proc. Natl. Acad. Sci. U.S.A.* **2003**, *100*, 3695–3700.
(18) Rombach, M.; Seebacher, J.; Ji, M.; Zhang, G. F.; He, G. S.; Ibrahim, M. M.; Benkmil, B.; Vahrenkamp, H. *Inorg. Chem.* **2006**, *45*, 4571–4575.
(19) Tekeste, T.; Vahrenkamp, H. *Inog. Chim. Acta* **2007**, *360*, 1523–1528.
(20) Sienkiewicz, A.; Smith, B. G.; Veselov, A.; Scholes, C. P. *Rev. Sci. Instrum.* **1996**, *67*, 2134–2138.
(21) Usov, O. M.; Choi, P. S.; Shapleigh, J. P.; Scholes, C. P. *J. Am. Chem. Soc.* **2006**, *128*, 5021–32.
(22) Usov, O. M.; Chois, P. S.-T.; Shapleigh, J. P.; Scholes, C. P. *J. Am. Chem. Soc.* **2005**, *127*, 9485–9494.
(23) Usov, O. M.; Grigoryants, V. M.; Tagore, R.; Brudvig, G. W.; Scholes, C. P. *J. Am. Chem. Soc.* **2007**, *129*, 11886–7.
(24) Usov, O. M.; Sun, Y.; Grigoryants, V. M.; Shapleigh, J. P.; Scholes, C. P. *J. Am. Chem. Soc.* **2006**, *128*, 13102–11.

ENDOR spectra are the sum of separate sweeps in both directions to avoid distortions from internal spin relaxation. The overall uncertainty in ENDOR frequencies is approximately ±0.1−0.3 MHz. It should be noted that ENODR of this hs Co(II) series requires approximately 100-fold more microwave power to saturate the electron spin system than was necessary in many of our preceding studies.[21−24] As the rf-induced ENDOR effect is in competition with electron spin relaxation, one may expect lower ENDOR sensitivity under such high power conditions.

First-Order ENDOR. For a single molecular orientation with respect to the applied field, the frequencies of proton ENDOR features center, to first order, at the free proton Larmor (nuclear Zeeman) frequency, ν_H. At Q-band (ν_e = 34.1 GHz), when, $g_{||}$ = 8.5 (2860 G), ν_H occurs at 12.2 MHz. The hyperfine coupling (A_H), representing the energy of interaction between the electron and nuclear spins, splits the nuclear spin doublet away from ν_H by ±1/2A_H for protons coupled to the electron spin ±1/2 doublet. Proton ENDOR frequencies occur as "ν^+" or "ν^-" branches, as shown in eq 1.[25]

$$\nu_H^{\pm} = \left|\nu_H \pm \frac{A_H}{2}\right| \tag{1}$$

A distinguishing feature of proton ENDOR is that, when $\nu_H > A/2$, the proton ENDOR frequencies increase with ν_H as the magnetic field increases. Under rapid-passage conditions, it is common for the predicted $\nu^{\pm}$ features to show unequal intensity in CW ENDOR.[21,22,25,26] For the present work, it was sufficient for assignment and for computation of proton hyperfine couplings to observe only one of the Zeeman partners. The proton couplings are largely determined by Co(II)···H through-space dipolar coupling. The position and orientation of the protons, nitrogens, and borons, relative to the Co(II) ion and its **g**-tensor are known from our previous studies,[10] and thus the signs of individual dipolar couplings are known. In general, for protons that have positive dipolar couplings only, the ν^+ resonance, above the free proton frequency, was observed, while for protons that have negative dipolar couplings, only the ν^- resonance, below the free proton frequency, was seen. A consistent, though not definitive, explanation for both occurrences is that the CW rapid-passage ENDOR signal arises from excitation of the protons in the electronic $S_z = -1/2$ ground manifold, rather than in the excited $S_z = +1/2$ manifold, possibly due to operation at temperatures at or below 2 K.

$$\nu_N^{\pm} = \left|\frac{A(^{14}N)}{2} \pm \nu_N \pm \frac{3P(^{14}N)}{2}\right| \tag{2}$$

The first-order expressions for strongly coupled ^{14}N (I = 1) ENDOR frequencies are given by eq 2.[25] In eq 2, $A(^{14}N)$ is the hyperfine coupling, P is the ^{14}N quadrupolar coupling, and ν_N (= 0.9 MHz at 2860 G) is the ^{14}N nuclear Zeeman frequency. It is particularly common in CW ENDOR studies of ^{14}N, under rapid passage conditions at Q-band, to observe only the ν^+ features from strongly coupled ^{14}N.[22,27−31] For I = 3/2 ^{11}B, the first-order ENDOR expressions are given by eq 3.[25] In eq 3b, $A(^{11}B)$ is the ^{11}B hyperfine coupling, $P(^{11}B)$ is the ^{11}B quadrupolar coupling, and ν_B (=3.9 MHz at 2860 G) is the ^{11}B Larmor frequency.

$$\nu_B^{+} = \left|\frac{A(^{11}B)}{2} + \nu_B \pm \frac{3P(^{11}B)}{2}\right| \quad \text{and} \quad \left|\frac{A(^{11}B)}{2} + \nu_B\right| \tag{3a}$$

$$\nu_B^{-} = \left|\frac{A(^{11}B)}{2} - \nu_B \pm \frac{3P(^{11}B)}{2}\right| \quad \text{and} \quad \left|\frac{A(^{11}B)}{2} - \nu_B\right| \tag{3b}$$

Magnetic Ground State of Co(II) in Co(Tp)$_2$. With experimental data at both $g_{||}$ (Q-band, *vide infra*) and $g_{\perp}$ (X-band),[10] a more complete evaluation of the proton and nitrogen hyperfine tensors can be performed. A brief re-examination of the ground state electronic structure of Co(II) in D_{3d} symmetry, based on the prior work of Abragham and Pryce,[3,4] Jesson,[6−9] and McGarvey[13] is presented here.

For Co(II) in Co(Tp)$_2$, the $^4T_{1g}$ ground state of the pseudo-octahedral cobalt ion is split by a trigonal distortion, resulting in overall D_{3d} symmetry, with the trigonal axis oriented along the B···Co···B vector (see Figure 1). The lowest lying states in D_{3d} are an orbital singlet, $^4A_{2g}$, and an orbital doublet, ^4E_g. The singlet and the doublet are separated by the trigonal splitting parameter, δ. The corresponding d-orbital energy level diagram in Figure 2 shows the spin population of the metal d orbitals for the $^4A_{2g}$ and ^4E_g states. Both $^4A_{2g}$ and ^4E_g have unpaired spin in their d_{z^2} and $d_{x^2-y^2}$ orbitals (where "x", "y", "z" refer to the original octahedral axes), but differ in the population of their dπ orbitals. These latter dπ orbitals are shown as linear combinations of the original octahedral d_{xy}, d_{yz},and d_{xz} orbitals, where these linear combinations transform as basis functions for the A_{2g} and E_g irreducible representations of the D_{3d} point group.

To facilitate angular momentum and g-value calculations on hs Co(II) states, Abragam and Pryce[4] introduced the concept of a fictitious angular momentum operator, L', which has a similar matrix representation within the $^4T_{1g}$ manifold to that of a P state ($|1\rangle$, $|0\rangle$, and $|-1\rangle$).[4,6] The relation between the true (unprimed) angular momentum operators and the primed operators is that $L_{x,y} = -\gamma' L'_{x,y}$ and $L_z = -\gamma L'_z$, where the operator L' has effective Landé factors $-\gamma$ and $-\gamma'$ in the axial and perpendicular directions, respectively. The effective P states are given by eq 4. The combination of spin−orbit coupling and the trigonal distortion leaves six effective spin 1/2 Kramers doublets, each with its own g-values and energies.[6,13] The six doublets are shown schematically by the additional splittings under the double group notation D_{3d}* in Figure 2.

$$\begin{aligned} |1\rangle &= -\frac{(E_g^x + iE_g^y)}{\sqrt{2}} \\ |0\rangle &= (A_{2g}) \\ |-1\rangle &= \frac{(E_g^x - iE_g^y)}{\sqrt{2}} \end{aligned} \tag{4}$$

The ground state wave function is found by diagonalizing the combined spin−orbit and trigonal Hamiltonian, given by the 3 × 3 matrix of eq 5.[4,6] This Hamiltonian operates on the states $|-1, 3/2\rangle$, $|0, 1/2\rangle$, and $|1, -1/2\rangle$, which are the effective spin doublet states including orbital character. The spin−orbit coupling constant, λ, is negative in sign for d^7 Co(II), and δ is the energy of the trigonal distortion from Figure 2.

(25) Hoffman, B. M.; DeRose, V. J.; Doan, P. E.; Gurbiel, R. J.; Houseman, A. L. P.; Telser, J. In *Biological Magnetic Resonance, Vol. 13: EMR of Paramagnetic Molecules*, Berliner, L. J., Reuben, J., Eds.; Plenum: New York, 1993; Vol. 13.

(26) Werst, M. M.; Davoust, C. E.; Hoffman, B. M. *J. Am. Chem. Soc.* **1991**, *113*, 1533–1538.

(27) Fann, Y.-C.; Gerber, N. C.; Osmulski, P. A.; Hager, L. P.; Sligar, S. G.; Hoffman, B. M. *J. Am. Chem. Soc.* **1994**, *116*, 5989–5990.

(28) Lee, H. I.; Dexter, A. F.; Fann, Y. C.; Lakner, F. J.; Hager, L. P.; Hoffman, B. M. *J. Am. Chem. Soc.* **1997**, *119*, 4059–4069.

(29) Rocklin, A. M.; Tierney, D. L.; Kofman, V.; Brunhuber, N. M. W.; Hoffman, B. M.; Christoffersen, R. E.; Reich, N. O.; Lipscomb, J. D.; Que, L. *Proc. Natl. Acad. Sci. U.S.A.* **1999**, *96*, 7905–7909.

(30) Tierney, D. L.; Rocklin, A. M.; Lipscomb, J. D.; Que, L.; Hoffman, B. M. *J. Am. Chem. Soc.* **2005**, *127*, 7005–7013.

(31) Veselov, A. V.; Osborne, J. P.; Gennis, R. B.; Scholes, C. P. *J. Am. Chem. Soc.* **2000**, *122*, 8712–8716.

$$\begin{bmatrix} \frac{3}{2}\gamma\lambda & -\sqrt{\frac{3}{2}}\gamma'\lambda & 0 \\ -\sqrt{\frac{3}{2}}\gamma'\lambda & \delta & -\sqrt{2}\gamma'\lambda \\ 0 & -\sqrt{2}\gamma'\lambda & \frac{1}{2}\gamma\lambda \end{bmatrix} = 0 \quad (5)$$

$$\Psi^{\pm 1/2} = a|\mp 1, \pm 3/2\rangle + b|0, \pm 1/2\rangle + c|\pm 1, \mp 1/2\rangle \quad (6)$$

The ground state doublet responsible for the hyperfine couplings measured by ENDOR will have wave functions that take the form of eq 6. Electronic g-values are then obtained by evaluating the operators $2(g_e S_z - \gamma L'_z)$ to find $g_{\|}$ and $2(g_e S_x - \gamma' L'_x)$ to find $g_{\perp}$. The resulting g-values are given by eq 7. EPR and optical spectroscopy[6,13] yield the following values: $\lambda = -146.7$ cm^{-1}, $\delta = 1900$ cm^{-1}, $\gamma = 1.434$, $\gamma' = 1.379$. These parameters, in turn, lead to coefficients of $a = 0.98$, $b = -0.13$, and $c = 0.15$ in eq 6. The implication of a coefficient near unity for the $|\mp 1, \pm 3/2\rangle$ doublet is that the ground state is essentially an $S_z = 3/2$ state with -1 unit of angular momentum.

$$g_{\|} = (6a^2 + 2b^2 - 2c^2) + 2\alpha(a^2 - c^2) \quad (7a)$$

$$g_{\perp} = (4b^2 + 4\sqrt{3}ac) - \sqrt{8}\alpha' bc \quad (7b)$$

Behavior of the Fermi Coupling. The Fermi (or contact) coupling, $A_{iso}\mathbf{I}\cdot\mathbf{S}$, is intrinsically isotropic, and it will appear so if the electronic spin distribution has expectation values of $\langle S_x\rangle$, $\langle S_y\rangle$, and $\langle S_z\rangle$, which are equal to each other. However, when the Fermi coupling is evaluated within the effective spin $\pm 1/2$ ground state wave function of eq 6, which has very different expectation values for $\langle S_x, S_y\rangle$, and $\langle S_z\rangle$, the Fermi interaction becomes an anisotropic tensor, $A_{\|,\mathrm{Fermi}} I_z S_z + B_{\perp,\mathrm{Fermi}}(I_x S_x + I_y S_y)$. Using the values of the orbital coefficients a, b, and c given above,[6,13] the apparent Fermi couplings are predicted to be ca. 5-fold larger in the parallel direction than in the perpendicular direction (eq 8).

$$A_{\|,\mathrm{Fermi}} = A_{iso}(3a^2 + b^2 - c^2) = 2.88A_{iso} \quad (8a)$$

$$B_{\perp,\mathrm{Fermi}} = A_{iso}(2b^2 + 2\sqrt{3}ac) = 0.54A_{iso} \quad (8b)$$

$$A(^{14}\mathrm{N})_{\mathrm{Fermi}} = A(^{14}\mathrm{N})_{iso}\left[\left(\frac{2.88g_{\|}\cos\theta}{g_{\mathrm{eff}}}\right)^2 + \left(\frac{0.54g_{\perp}\sin\theta}{g_{\mathrm{eff}}}\right)^2\right]^{1/2} \quad (9)$$

As explained through eq 8, the Fermi coupling is rendered effectively anisotropic by the unusual Co(II) ground state wave function. When the anisotropic Fermi coefficients of eq 8b are used to evaluate the hyperfine Hamiltonian (eq S4 in Appendix I of the Supporting Information), a highly angle-dependent Fermi coupling results for ^{14}N (eq 9). A plot of the angular dependence of eq 9 is provided in the Supporting Information (Figure S1), which shows that over the range of $\theta = 0°-70°$ (with respect to the applied field) $A(^{14}\mathrm{N})_{\mathrm{Fermi}}$ decreases from its maximum value by only 5%.

$$A_{\mathrm{Dip}} = \frac{3(\mu_e\mathbf{R})(\mu_H\mathbf{R})}{r^5} - \frac{(\mu_e\mu_H)}{r^3} \quad (10)$$

Behavior of the Dipolar Proton Hyperfine Coupling. The observed hyperfine coupling is a sum of Fermi and dipolar terms, the latter given by the general expression in eq 10. For the pyrazolyl protons, the dipolar term represents the largest contribution to the observed hyperfine coupling and is expected in most cases to be largest near the $g_{\|}$ axis because of the exceptionally large value of $g_{\|}$. In eq 10, $\mathbf{R}$ is the metal−proton vector, r is the metal−proton distance, $\mu_e = \beta_e(g_{\|}S_z + g_{\perp}S_x + g_{\perp}S_y)$ is the electronic magnetic moment, which includes orbital angular momentum, and $\mu_H = g_H\beta_n(I_z + I_x + I_y)$ is the proton nuclear magnetic moment. As illustrated in Figure 1, the hyperfine tensors of the BH ($\theta = 0°$) and 3H ($\theta \approx 90°$) protons are essentially collinear with the Co(II) ion's **g**-tensor, and this affords narrow ENDOR lines near $g_{\|}$. For both 3H and BH, because of the large g-anisotropy, $A_{z,\mathrm{dip}}$ is roughly 8.5 times larger than $A_{x,\mathrm{dip}}$ and $A_{y,\mathrm{dip}}$. Relatively small through-bond contact interactions will simply add small increments to all three, and these are only resolved at the g-value extrema, where spectral resolution is greatest. The terms in the dipolar Hamiltonian which provide first-order perturbation to the electron spin levels are those that are collinear with S_z'. These first-order terms, and the angle-dependent ENDOR couplings they predict for the BH and 3H protons, are derived and presented graphically in Appendix II of the Supporting Information, Figures S2 and S3. The dipolar

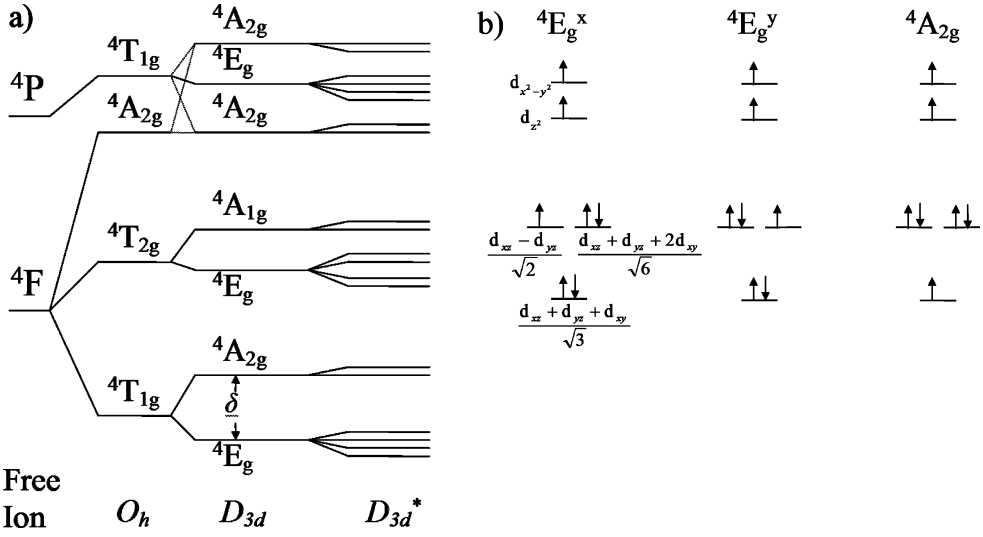

Figure 2. (a) Energy level diagram (arbitrary scale). The extent of trigonal distortion is given by the parameter δ. Addition of spin−orbit coupling yields a series of E_g states, D_{3d}*. (Reproduced with permission from ref 6. Copyright 1966 American Institute of Physics.) (b) The configuration of d-electrons in the ligand field scheme that gives rise to the E_g^x, E_g^y, and A_{2g} configurations. The appropriate linear combinations of the original of d_{xy}, d_{yz}, and d_{xz} orbitals, which properly transform as A_{2g} and E_g under D_{3d} symmetry, are shown.

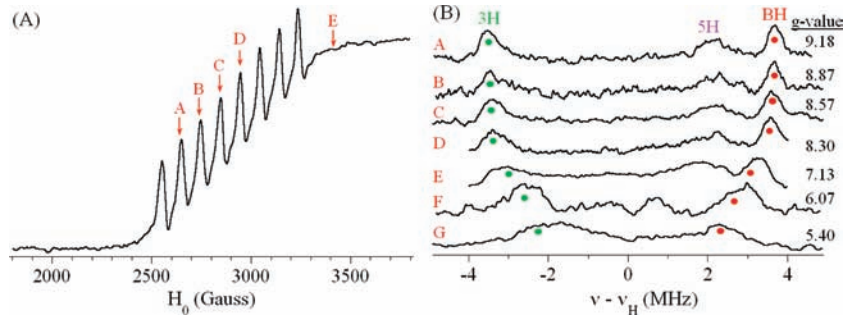

Figure 3. (A) Q-band (34.1 GHz) dispersion rapid-passage EPR spectrum at 2 K. Positions A (H_0 = 2430 G), B (2540 G), C (2630 G), D (2740 G), and E (3400 G) correspond to field positions where ENDOR spectra were taken. (B) Q-band CW proton ENDOR spectra taken at progressively higher fields [A−E as indicated in A, F (4000 G) and G (5000 G)]. The splittings of the two major features diminish approximately as the cosine of θ, as illustrated (see Discussion,and Appendix II of the Supporting Information) with green (3H) and red (BH) markers. Conditions: T = 2 K, microwave power 9.0 μW, dispersion detection, 2.6 G (100 kHz) field modulation, 20 W rf power (10% duty cycle, 100 μs on/900 μs off), 10 MHz/s rf sweep rate.

splittings for these two protons are predicted to follow $\approx A_{z,dip}$ cos θ over the range $\theta = 0°-70°$ with respect to the applied field. The angular dependence of the dipolar coupling for the 5H proton (θ = 33°) is more complicated, with a large orientation-dependent variation in proton hyperfine couplings and a resultant broadly dispersed powder pattern (see Figures S4 and S5, Supporting Information).

Results

EPR-ENDOR Spectroscopy. The X-band EPR spectrum of $Co(Tp)_2$ (Figure 1C) spans nearly 7200 G. The high-field derivative provides an estimate of $g_\perp$ and the low-field feature bears well-resolved ^{59}Co (I = 7/2) hyperfine splitting centered at $g_{||}$. The Q-band dispersion rapid-passage spectrum (Figure 3A) details the $g_{||}$ region with its large ^{59}Co hyperfine splitting of 93 G. The best-resolved ENDOR spectra were taken nearest the $g_{||}$ extremum (position "A" in Figure 3A), which will for many nuclei present well-resolved "single-crystal-like" ENDOR spectra.[32] Because of the large g-value anisotropy, the underlying EPR intensity in the $g_{||}$ region, on which the ENDOR signal depends, is small. Consequently, while the relatively large EPR signal at $g_\perp$ afforded easy ENDOR detection at X-band (at a g-value that, at Q-band, corresponds to B_0 = 2.8 T, a field inaccessible to most electromagnets),[10] the greater sensitivity of rapid-passage Q-band ENDOR at pumped helium temperatures was required to obtain reliable spectra near $g_{||}$.

Proton ENDOR. Figure 3B shows field-dependent Q-band proton ENDOR spectra of $Co(Tp)_2$ from the low-field (high-g) edge of the EPR spectrum to just above the last ^{59}Co hyperfine line (field positions correspond to points A−E in Figure 3A) and beyond. The BH and 3H signals displayed adequate resolution and signal-to-noise to be tracked from the $g_{||}$ edge of the $Co(Tp)_2$ EPR spectrum to $g \sim 5.4$; observed hyperfine couplings are summarized in Table 1. Only one of the two expected ^{1}H lines was observed per proton (see Materials and Methods). As illustrated in Figure 3B, the field-dependence of the of the BH and 3H proton hyperfine couplings follow cos θ with respect to the applied field (red and green markers in Figure 3B). This behavior is well-reproduced in field-dependent ENDOR simulations that incorporate the coupling parameters in Table 1, including the small anisotropic Fermi couplings, as well as the relatively larger dipolar couplings (see Figure S6, Supporting Information). However, it is important to note that the best resolution of small corrections to the predicted hyperfine couplings, such as those associated with anisotropy in the Fermi coupling, are best elucidated at the g-value extrema. The observed cos θ dependence is a direct result of the large electronic g-anisotropy, which forces the alignment of the internal hyperfine field with the $g_{||}$ axis, while the applied magnetic field, which quantizes the nuclear spin, occurs at an ever increasing angle, θ, to the $g_{||}$ axis (see Appendix II, Supporting Information).

Table 1. ENDOR-Determined ^{14}N, ^{11}B, and ^{1}H Hyperfine Couplings in $Co(Tp)_2$[a]

			Q-Band			X-Band			
atom	R[b]	θ[b]	$\lvert A_{\|\|,obs}\rvert$	$A_{z,dip}$[c]	ΔA[d]	$A_{\perp,obs}$[e]	$A_{\perp,dip}$[c]	A_{iso}[f]	f_{Co}
				$Co(Tp)_2$					
2-^{14}N	2.16	52	34	~0		6		11.8	
^{11}B	3.20	0	5.8	6.6	−0.9	−0.3	−0.4		
3H	3.44	84	7.1	−8.0	+0.9	2.0	1.9[g]	+0.17	0.96
						0.9	−1.0[h]		
BH	4.35	0	7.2	8.1	+0.9	0.6	−0.5	−0.29	0.99
5H	5.04	33	~3.5[i]	<5.2	n/a				
				$Co(Tp^{3Me})_2$					
2-^{14}N									
3Me	3.73	92	5.3	−6.6	+1.3				
				$Co(n\text{BuTp})_2$					
2-^{14}N									
3H	3.33	86	7.6	−8.9	+1.3				
α-CH_2	5.25	7	3.8	4.5	−0.7				

[a] All couplings (A) reported in MHz, ±0.1−0.3. [b] Co(II)−nucleus distance (R) in Å, and angle (θ in deg) between the metal−nucleus vector and the $g_{||}$ (B···Co···B) axis, from Myers et al.[10] [c] In general, $A_{dip} = (g_{eff}g_n\beta_e\beta_n)/(hR^3)(3\cos^2\theta - 1)$, assuming 100% of the spin on the Co(II) ion (f_{Co} = 1.00), where g_n is the relevant nuclear g-factor, and β_e and β_n take their usual values. In calculating $A_{z,dip}$, $g_{eff} = g_{||} = 8.48$; in calculating $A_{\perp,dip}$ ($A_{x,dip}/A_{y,dip}$), $g_{eff} = g_\perp = 1.02$. [d] Difference between $\lvert A_{||,obs}\rvert - A_{z,dip}$, assuming that A_{obs} has the same sign as $A_{z,dip}$. [e] From Myers et al.[10] [f] Value of A_{iso} for pyrazolyl 2-^{14}N; see Discussion. Values of A_{iso} and f_{Co} derive from least-squares analysis outlined in Appendix III of the Supporting Information. [g] Appropriate value of θ for $A_{||}$ in the $g_\perp$ plane for this proton is 6°. [h] Appropriate value of θ for $A_\perp$ in the $g_\perp$ plane for this proton is 90°. [i] Approximate value of $A_{||}$ from the center of the powder pattern observed at $g_{||}$; see Figure 3B and Appendix II of the Supporting Information for details.

The Co(II)···4H and Co(II)···5H vectors make angles of 61° and 33°, respectively, with the $g_{||}$ axis. Being significantly off-axis, the 4H and 5H protons will exhibit broadened ENDOR spectra, even at the $g_{||}$ extremum.[32] As the Co(II)···4H vector lies close to the magic angle, it is expected to display little dipolar coupling at $g_{||}$, and no resolved features were observed that could be ascribed to the 4H protons. Near $g_{||}$, the feature assigned to the 5H proton (see Figure 4B) is ~1.5 MHz in width (fwhm), compared to ~0.3 MHz for the 3H proton. Theoretical

(32) Hoffman, B. M.; Gurbiel, R. J. *J. Magn. Reson.* **1989**, *82*, 309–317.

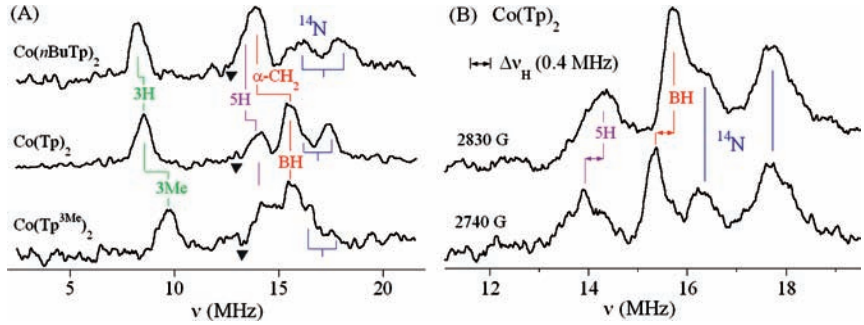

Figure 4. (A) ENDOR spectra taken near $g_{||}$ for Co(nBuTp)$_2$, Co(Tp)$_2$, and Co(Tp^{3Me})$_2$. The brackets indicate the shift of peak positions that accompanies a given structural perturbation; the inverted triangles mark ν_H. (B) Distinction of ^{1}H features from overlapping ^{14}N, which are insensitive to changing the magnetic field from 2740 G (point D in Figure 3A) to 2830 G. Proton features are shifted ~0.4 MHz to higher frequency, equal to the change in ν_H. Conditions: In A, H = 2822, 2830, and 2895 G for Co(Tp)$_2$, Co(nBuTp)$_2$, and Co(Tp^{3}Me)$_2$, respectively. All other conditions, in both A and B, as in Figure 3.

expressions and detailed spectral simulations describing the broadened ENDOR response of the 5H proton are presented in the Supporting Information, Figures S4 and S5.

The assignments in Figure 3B were obtained by comparison of the ENDOR features of the parent compound with those of a set of selectively substituted analogs, as shown in Figure 4. Figure 4A compares ENDOR of Co(Tp)$_2$, Co(nBuTp)$_2$, and Co(Tp^{3Me})$_2$ (see Figure 1B). Analogous to our previous use of selective substitutions to examine the relative contributions to NMR chemical shifts,[10] the substitution of protons by methyl or alkyl groups is expected to attenuate the hyperfine coupling relative to the corresponding protons of Co(Tp)$_2$. Since only one type of proton was changed at a time, each substitution should then result in the disappearance of that proton feature in Figure 4A and its replacement by a feature of smaller coupling. For example, the 7.1 MHz coupling of the 3H proton in Co(Tp)$_2$ (Table 1) was reduced to 5.3 MHz for the 3Me protons in Co(Tp^{3Me})$_2$. Similarly, the 7.2 MHz coupling of the BH proton in Co(Tp)$_2$ was reduced to 3.8 MHz for the α-CH$_2$ protons of the n-butyl group in Co(nBuTp)$_2$. A measurable decrease of about 0.3 MHz in frequency (corresponding to an increase of ~ 0.6 MHz in hyperfine coupling) was also observed for the 3H proton of Co(nBuTp)$_2$, where crystallography indicates a concomitant 3% decrease in the Co(II)···3H distance in Co(nBuTp)$_2$ relative to Co(Tp)$_2$. It should be noted that the lines assigned to 3H and BH cannot be assigned as the ν^+/ν^- pair of a single proton (see Supporting Information, Figure S7).

^{14}N ENDOR. Two features to high frequency of the BH proton (labeled ^{14}N in Figure 4A) showed almost no field-dependence, as shown in Figure 4B. The two spectra, taken at fields that differ by 90 G, show two features assigned to the 5H and BH protons that shift by ~0.4 MHz, the expected change in ν_H. In contrast, the corresponding change in the ^{14}N nuclear Zeeman frequency is only 0.03 MHz ($(g_n(^{14}N))/(g_n(^1H)) \sim 0.07$), and the two field-independent features in Figure 4B can therefore be assigned to the coordinating pyrazolyl 2-N nitrogens, and examination of Figure 4A shows that the ^{14}N coupling in the three structural analogs is similar. The variations in ^{14}N couplings that are observed can easily be attributed to subtle differences in Co−N bond lengths and bite angles.[10]

The peak separation of ~1.5 MHz in Figure 4B may reflect the ^{14}N quadrupole coupling[33] or the nuclear Zeeman splitting of $2\nu(^{14}N) = 1.7$ MHz. In the latter case, the two ^{14}N features

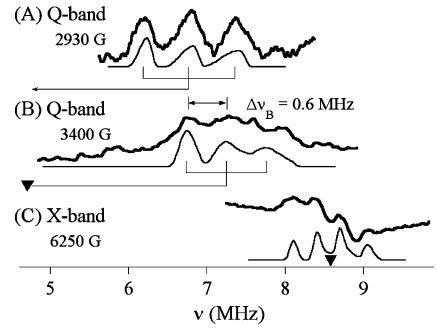

Figure 5. ^{11}B ENDOR spectra (bold lines) from Co(Tp)$_2$ and representative simulations (thin lines). (A) ν_e = 34.1 GHz, H = 2930 G (g = 8.20). (B) ν_e = 34.1 GHz, H = 3400 G (g = 7.14). (C) ν_e = 9.4 GHz, H = 6250 G (g = 1.08), from Myers et al.[10] The brackets are meant to guide the reader, representing the three ν^+ features expected for ^{11}B near $g_{||}$, in A and B (See eq 3a); the inverted triangles in B and C mark ν_B, which occurs at 4.0 MHz in A. Conditions for A and B: 2 G field modulation, 3 MHz/s rf sweep rate; all other conditions as in Figure 3. GENDOR[55] simulation parameters: g [8.48, 1.02, 1.02], A [5.8, −0.33, −0.33], P [0.2, −0.1, −0.1], 200 G EPR line width, 0.05 MHz ENDOR line width, 100 integration points over an integration interval of 100.

would correspond to both ν^+ and ν^-, with unresolved quadrupole couplings of $P < 0.2$ MHz (2/3 fwhm of the nitrogen features, corresponding to the limiting value of $3/2P$; see eq 2) and a ^{14}N hyperfine coupling of 34 MHz. The alternative description, assigning the two features as the coordinating nitrogen's ν^+ quadrupole pair, without observation of ν^-, is more consistent with the expectation that only ν^+ will be observed,[22,27−31] and corresponds to a ^{14}N hyperfine coupling of 32 MHz with P = 1.0 MHz. A series of spectra collected to $g \sim 3.5$ (~7000 G, Supporting Information, Figure S8) more fully distinguished these features, whose frequency stayed nearly constant at 17−18 MHz, while the overlapping proton features moved from lower to higher frequency with respect to them. The magnitude of the ^{14}N hyperfine coupling, and its insensitivity to applied field, is consistent with its source being the Fermi coupling from 2s spin in the nitrogen σ antibonding orbital.

^{11}B ENDOR. Near $g_{||}$ a well-resolved triplet was observed at lower frequency from the 3H proton (Figure 5). A 570 G change in field, from 2930 (Figure 5A) to 3400 G (Figure 5B), is accompanied by a shift to higher frequency of ~0.6 MHz, consistent with the expected change in ν_B. Thus, we assign this three-line pattern to the quadrupole-split ν^+ feature of the apical $I = 3/2$ ^{11}B, as predicted by eq 3a. The pattern of Figure 5A centers at $|A/2 + \nu_B|$, giving A = 5.8 MHz. The quadrupole splitting, $|P_{||}(^{11}B)|$, in the direction of the trigonal distortion is

(33) Scholes, C. P.; Lapidot, A.; Mascarenhas, R.; Inubushi, T.; Isaacson, R. A.; Feher, G. *J. Am. Chem. Soc.* **1982**, *104*, 2724–2735.

0.2 MHz. Because $A/2$ and ν_B are nearly equal at the fields employed, the ^{11}B ν^- feature occurs at very low frequency and was not observed. In our previous X-band ENDOR studies at $g_\perp$,[10] a set of four features centered at the ^{11}B NMR frequency was observed (Figure 5C). The set of thin lines in Figure 5 shows that the X-band ^{11}B features at $g_\perp$, together with the Q-band ^{11}B features at $g_\parallel$, can be simulated using a single set of dipolar hyperfine and quadrupole coupling parameter values (Table 1).

Discussion

Proton Hyperfine Couplings. As $A_{z,dip}$ (eqs 10 and S5, S6, and S8, Supporting Information) depends on the large value of $g_\parallel$, the proton hyperfine couplings at $g_\parallel$ are expected to be dominated by dipolar coupling. The experimentally determined hyperfine couplings are similar in magnitude to predicted dipolar contributions (Table 1), consistent with this expectation. The observed couplings also proved quite sensitive to even a small change in metal-to-proton distance. A 0.3 MHz change in frequency is observed when the 3H distance changes from 3.44 Å in the parent complex $Co(Tp)_2$ to 3.33 Å in $Co(n\text{BuTp})_2$. The Co(II)···4H and Co(II)···5H vectors are well off the $g_\parallel$ axis, and the breadth of their features precludes more detailed analysis (see Figures S4 and S5, Supporting Information). The best resolved couplings are those from the 3H and BH protons, whose metal-to-proton vectors make respective angles of 0° and ~90° to the $g_\parallel$ axis. As such, $g_\parallel$ represents a principal hyperfine direction for each, giving "single-crystal-like" ENDOR at $g_\parallel$.[25,32]

The measured 3H and BH couplings are consistently smaller in magnitude than the calculated dipolar couplings. This difference (Table 1) may reflect (i) the contact interaction and/or (ii) the reduction of the dipolar term due to covalency, which reduces the total spin on Co(II). Treating the difference as entirely due to the contact interaction, $A_{\parallel,Fermi}$ (= 2.88 A_{iso}) in eq 4a, then the respective values of A_{iso} for the 3H and BH protons would be +0.29 and −0.34 MHz, which compare well with previous estimates from ambient temperature NMR (+0.45 and −0.23 MHz, respectively)[8] but differ substantially for the BH proton from our previous work (1.3 MHz).[10] This difference most likely reflects the presence of measurable contact interactions between the Co(II) ion and the methyl protons of $Co(Tp^{3Me})_2$ ($\Delta A = -0.7$ MHz in Table 1) and the α-CH_2 protons of $Co(n\text{BuTp})_2$ ($\Delta A = +1.3$ MHz in Table 1). The α-CH_2 and 3Me protons were assumed to have zero isotropic coupling in our original analysis, and this assumption was sufficient to simulate the small ^1H ENDOR couplings at $g_\perp$.[10]

For the 3H proton there was sufficient ENDOR information from a combination of this work at $g_\parallel$ and our previous work at $g_\perp$[10] to provide independent estimates of the anisotropic Fermi couplings and the fraction of spin that resides on the Co(II) ion, f_{Co}, reflected in the magnitude of the dipolar couplings (see eq S8, Supporting Information). Three separate ENDOR frequencies that are functions of both the anisotropic dipolar coupling (eqs 10 and S5, S6, and S8, Supporting Information) and the anisotropic contact interaction (eq 8) were available. These frequencies, provided in Table 1, are the hyperfine coupling measured by Q-band ENDOR at $g_\parallel$ [(−)7.10 MHz], and two values measured by X-band ENDOR in the $g_\perp$ plane [(+)1.97, (−)0.92 MHz]. The relevant X-band spectra at $g_\perp$, marking the features germane to this analysis, are provided in Supporting Information, Figure S9. The first X-band feature [(+)1.97 MHz] is nearly parallel to the metal−proton vector, and the second [(−)0.92 MHz] is perpendicular to it.

With three frequencies, but only two parameters, f_{Co} and A_{iso}, necessary to fit the data, a least-squares procedure (details of the procedure are given in Appendix III of the Supporting Information) was used to obtain best fit values of $f_{Co} = 0.96 \pm 0.02$ and $A_{iso} = 0.17 \pm 0.05$ MHz for the 3H proton. This value for f_{Co} is consistent with previous analyses of ^{59}Co hyperfine couplings, which used an orbital reduction factor of about 0.9.[5,6] When the f_{Co} correction to the dipolar interaction plus the anisotropic Fermi interaction (eq 8) were both incorporated into a fit to A_{xx}, A_{yy}, and A_{zz} (see eqs S9, S10, and S11, Supporting Information), the sum of square errors (χ^2) between experimental and predicted values of A_{zz}, A_{xx}, and A_{yy} was diminished by over 200-fold from the uncorrected situation, based on estimated crystallographic values of $A_{z,dip}$, $A_{x,dip}$, and $A_{y,dip}$ with $f_{Co} = 1.00$ and no Fermi contact interaction. A Fermi interaction that is truly isotropic gives a 5-fold poorer fit relative to the anisotropic case of eq 8. The contact interaction derived from our least-squares analysis, which includes the anisotropic Fermi interaction (Table 1), is still of the same sign as that obtained by Jesson,[8] though smaller. The implication of a small positive contact interaction for the 3H proton, which is an α proton on an α carbon, is that covalent transfer of spin to the 3H proton does not occur through the ring π-system, because covalent transfer through the π-system would lead to a negative coupling for the 3H proton.[34] Spin is most likely directly transferred through the σ antibonding system to the 3H proton. As such the present study lends further support to the description of the trispyrazolylborate ligand as a purely σ donor, with minimal interaction with the metal ion through its π system.[35,36]

The BH proton is about 1 Å further from the metal than the 3H proton and lies with its metal−proton vector parallel to the $g_\parallel$ direction. Its smaller dipolar couplings, $A_{x,dip}$ and $A_{y,dip}$, are expected to be about −0.5 MHz at $g_\perp$. A feature with coupling of 0.64 MHz (Figure S9, Supporting Information), was previously ascribed to the BH proton.[10] From the two ENDOR frequencies for the BH proton, (+)7.20 MHz at $g_\parallel$ and (−)0.64 MHz at $g_\perp$, we estimate $f_{Co} = 0.99 \pm 0.03$ and $A_{iso} = -0.29 \pm 0.07$ MHz. The value of A_{iso} is comparable to that obtained by Jesson.[8]

Nitrogen Hyperfine Couplings. At Q-band, at all available fields, the observed ^{14}N ENDOR frequencies were essentially constant (Figure S8, Supporting Information). The prediction of eqs 8 and 9, shown graphically in Figure S1, Supporting Information, is that the ^{14}N Fermi coupling, which is expected to dominate the observed ^{14}N coupling, will be invariant to within 5% from $g_\parallel$ to $g \sim 3$. Thus, 34 MHz = 2.88 $A(^{14}N)_{iso}$ and $A(^{14}N)_{iso} = 11.8$ MHz. Equations 8b and 9 also predict that, in the $g_\perp$ plane, the effective Fermi hyperfine coupling is $B_{\perp Fermi} = 0.54$, and $A(^{14}N)_{iso} = 6.4$ MHz. This agrees well with our previous results at X-band,[10] which indicated an intrinsic ^{14}N hyperfine coupling of 6 MHz at $g_\perp$.

The metal d_{z^2} and $d_{x^2-y^2}$ orbitals of $Co(Tp)_2$ are disposed to transfer spin to the 2-N σ antibonding sp^2 orbitals which have 2s and 2p character.[37] If there are comparable amounts of spin with 2s and 2p character, the Fermi coupling to the 2s spin will

(34) McConnell, H. M.; Robertson, R. E. *J. Chem. Phys.* **1958**, *29*, 1361–1365.
(35) Fujihara, T.; Schonherr, T.; Kaizaki, S. *Inorg. Chim. Acta* **1996**, *249*, 135–141.
(36) Larrabee, J. A. A. C. M.; Asiedu, E. T.; Cook, J. O.; Hoerning, K. R.; Klingler, L. J.; Okin, G. S.; Santee, S. G.; Volkert, T. L. *J. Am. Chem. Soc.* **1997**, *119*, 4182–4196.
(37) Owen, J.; Thornley, J. H. M. *Rep. Prog. Phys.* **1966**, *29*, 675–728.

be at least an order of magnitude larger than the dipolar coupling to the 2p.[38,39] Compared to the original octahedral configuration, the perturbation of Co−N bond lengths and bond angles is minimal under D_{3d} symmetry (Figure 1A) so that all six pyrazolyl 2-N nitrogens remain equivalent.[10] Furthermore, the transferred spin from the original d_{z^2} and $d_{x^2-y^2}$ orbitals should be the same for each coordinating pyrazolyl nitrogen, as both of these orbitals are still populated with a single unpaired electron in D_{3d} symmetry (Figure 2). Thus, the Fermi coupling to each of the six equivalent pyrazolyl nitrogens is $A(^{14}N)_{iso} = 11.8$ MHz. Within the $S = 3/2$ manifold, $A(^{14}N)_{iso}$ can be related to the intrinsic Fermi coupling of an individual electron spin in its nitrogen σ antibonding orbital as follows: $A(^{14}N)_{Fermi} = (2S)A_{iso} = 35.4$ MHz.[37] This is substantially larger than the only other measurement available, the intrinsic hyperfine coupling of 21.6 MHz for Co(II)−$^{14}N_{His}$ in TFIIIA,[16] and may reflect inherent differences between Co(II)−N_{His} and Co(II)−$N_{pyrazole}$ bonding. However, the 35.4 MHz intrinsic coupling measured here yields unpaired electron spin density $f_{2s} = 2.2\%$ of one spin in the 2s component of a 2-N σ antibonding orbital,[38] which compares favorably to $f_{2s} = 2.5\%$ in the corresponding nitrogen σ antibonding orbital of ferric heme[33] and 3.0% for Cu(II) tetraphenylporphyrin.[40]

For sp^2 hybridization it is expected that the 2s contribution will be accompanied by a 2p contribution, which will be ~4.4% 2p per nitrogen. Overall, it might roughly be expected that there is $6 \times (2.2 + 4.4) \approx 39.6\%$ of one unpaired electron delocalized from the Co(II) onto the pyrazolyl nitrogens via σ antibonding orbitals. In principle, there should also be hyperfine contributions from unpaired 2p electrons themselves and from the direct dipolar interaction of spin on the Co(II) with the nitrogen nucleus. Because the B···Co−N angle is 52°, the dipolar coupling of the pyrazolyl ^{14}N to the metal spin and to 2p spin in the σ antibonding orbitals will be essentially zero ($3\cos^2\theta - 1 = 0.14$). The composition of the dπ [d_{xy}, d_{xz}, d_{yz}] orbitals in D_{3d} (Figure 2B) is a linear combination of the original octahedral dπ orbitals, and it has been suggested that unquenched 2p(π) orbital angular momentum associated with a hs $S = 3/2$ d^7 state may lead to novel ligand hyperfine couplings due to overlap with the metal dπ orbitals.[41] However, such couplings are expected to be at least an order of magnitude smaller than the ^{14}N couplings reported here.[38]

Boron Hyperfine and Quadrupole Couplings. ^{11}B ENDOR of molecular species in solution is largely unknown,[10,42−45] although it has been heavily studied in association with defect centers in amorphous and crystalline solids.[46−51] In addition to a hyperfine coupling of about 5.8 MHz, a well-resolved quadrupole coupling $|P_{||}(^{11}B)| = 0.20$ MHz was observed at $g_{||}$ (Figure 5A). The four-line pattern previously observed at $g_\perp$ (Figure 5C),[10] together with the signals near $g_{||}$ reported here (Figures 5A,B), are simulated well with a single set of hyperfine and quadrupole parameters. The simulations (thin lines in Figure 5) show that the ^{11}B hyperfine couplings near $g_{||}$ and at $g_\perp$ are almost entirely dipolar in origin. The dipolar coupling of 0.33 MHz in the $g_\perp$ plane was an expected ~17 times smaller than at $g_{||}$ because of the electronic g-factor difference and the apical boron's position on the $g_{||}$ axis. Although dipolar coupling to the Co(II) clearly dominates the ^{11}B hyperfine couplings, a solely dipolar coupling underestimated the observed coupling by about 13%, possibly due to a small contact interaction and/or the transfer of electron spin away from the cobalt ion.

The splitting in the X-band spectrum, $|P_\perp(^{11}B)| = 0.10$ MHz (Figure 5C), defines an axial ^{11}B quadrupole tensor, directed along $g_{||}$ ($|P_{||}(^{11}B)| = 0.20$ MHz), where the quadrupole coupling along the parallel direction is twice the magnitude of the coupling in the perpendicular direction and opposite in sign. The four-line pattern at X-band, with larger intensity of the two inner features is the result of approximately equal hyperfine ($A_{xx} = A_{yy} = -0.33$ MHz) and quadrupole ($3|P_\perp(^{11}B)| = 0.30$ MHz) splittings. This value is the same as that reported for $Tp^{3,5Me}Mo(V)(O)(OPh)_2$ at the g_3 turning-point of the Mo(V) EPR spectrum.[45] The existence of a measurable, axially symmetric quadrupole coupling implies dissimilarity between the sp^3 B−H bond and the sp^3 B−C bonds, as a truly tetrahedral boron would exhibit no quadrupole coupling.[52] By the Townes-Dailey analysis[52,53] the quadrupole coupling can be empirically described in terms of differences in valence 2p electronic populations, within the sp^3 orbital scheme of the boron atom.

The axial quadrupole Hamiltonian is $\hat{H}_Q = (e^2Qq)/([4I(2I-1)])(3I_z^2 - I(I+1))$ where e^2Qq is the nuclear quadrupole coupling constant and $I = 3/2$ (see pp 36−37 of Lucken[52]). The quadrupole splitting measured by ENDOR (see Figure 5 and eq 3) is $3|P(^{11}B)|$, which gives $|e^2Qq| = 6|P(^{11}B)| = 1.20$ MHz, about one-half the value expected for trigonal sp^2 ^{11}B.[52] The Townes−Dailey analysis (see Chapter 12 of Lucken[52]) relates the observed quadrupole coupling, e^2Qq, to the quadrupolar contributions from individual 2p valence electrons, and to the atomic quadrupole moment for one 2p atomic electron, e^2Qq_0 (−5.39 MHz for ^{11}B).[52,54] When a is the electronic population in the sp^3 orbital of the B−H bond and b is the

(38) The Fermi coupling in MHz is related to the fraction of unpaired spin in a 2s orbital, f_{2s}, as follows: $^{14}A_{Fermi} = (16 \times 10^{-6}) f_{2s} g_n \beta_e \beta_n |\Psi_{o2s}|^2 \pi / (3h) = (1.59 \times 10^3) f_{2s}$ (MHz), where g_n is the ^{14}N nuclear g-value (=0.40347), β_e and β_n are the electron and nuclear Bohr magnetons, $|\Psi_{o2s}|^2 = 33.4 \times 10^{24}$ cm^{-3} (Hartree, D. R.; Hartree, W. *Proc. R. Soc. London, Ser. A.* **1949**, *193*, 299–304.) is the 2s wave function at the nitrogen nucleus, and h is Planck's constant.

(39) The anisotropic contribution from a 2p electron is related to the fraction of unpaired spin, f_{2p}, in that orbital as follows: $A_p = (4 \times 10^{-6}) f_{2p} g_n \beta_e \beta_n \langle r^{-3} \rangle_{2p} / (5h) = (48.1) f_{2p}$ (MHz), where $\langle r^{-3} \rangle_{2p} = 21.1 \times 10^{24}$ cm^{-3} (Hartree, D. R.; Hartree, W. *Proc. R. Soc. London, Ser. A.* **1949**, *193*, 299–304.) is the expectation value of r^{-3} for a nitrogen 2p orbital, and h is Planck's constant. The maximum anisotropic difference between orientations parallel and perpendicular to the direction of the 2p orbital would be $3A_p = 144.9$ MHz.

(40) Hoffman, B. M.; Brown, T. G. *Mol. Phys.* **1980**, *39*, 1073–1109.

(41) Van Kooten, J. J.; Sieverts, E. G.; Ammerlaan, C. A. J. *Phys. Rev. B* **1988**, *37*, 8949–8957.

(42) Kaim, W.; Lubitz, W. *Angew. Chem., Int. Ed.* **1983**, *22*, 892–893.

(43) Lichtblau, A.; Hausen, H. D.; Schwarz, W.; Kaim, W. *Inorg. Chem.* **1993**, *32*, 73–78.

(44) Lichtblau, A.; Kaim, W.; Schulz, A.; Stahl, T. *J. Chem. Soc., Perkin Trans. 2* **1992**, 1497–1501.

(45) Farley, R. D.; Hoefer, P.; Maher, J. P.; McCleverty, J. A.; Murphy, D. M.; Rowlands, C. C.; Ung, V. A.; Ward, M. D. *Magn. Reson. Chem.* **2002**, *40*, 683–686.

(46) Muller, R.; Feege, M.; Greulich-Weber, S.; Spaeth, J.-M. *Semicond. Sci. Technol.* **1993**, *8*, 1377–1384.

(47) Baranov, P. G.; Mokhov, E. N.; Hofstetter, A.; Sharmann, A. *JETP Lett.* **1996**, *63*, 803–808.

(48) Matsumoto, T.; Poluektov, O. G.; Schmidt, J.; Mokhov, E. N.; Baranov, P. G. *Phys. Rev. B (Cond. Matter)* **1997**, *55*, 2219–2229.

(49) Hong, W.; Chirila, M. M.; Garces, N. Y.; Halliburton, L. E.; Lupinski, D.; Villeval, P. *Phys. Rev. B: Cond. Matter Mater. Phys.* **2003**, *68* (1−9), 094111.

(50) Kordas, G. *Phys. Chem. Glasses* **2000**, *41*, 358–361.

(51) Kordas, G.; Goldfarb, D. *J. Chem. Phys.* **2008**, *129* (1−8), 154502.

(52) Lucken, E. A. C. *Nuclear Quadrupole Coupling Constants*; Academic Press Inc.: London, 1969.

(53) Townes, C. H.; Dailey, B. P. *J. Chem. Phys.* **1949**, *17*, 782–796.

(54) Wessel, G. *Phys. Rev.* **1953**, *92*, 1581–1582.

(55) The ENDOR simulation program GENDOR is available upon request from Prof. B. M. Hoffman, Department of Chemistry, Northwestern University.

corresponding population in the sp^3 orbital of a B−C bond, then $|(e^2Qq)/(e^2Qq_0)| = 3/4(a - b)$. Due to the lower electronegativity of hydrogen relative to carbon, a is expected to be larger than b (see Table 12.2 of Lucken[52]). The value of $|a - b| = 0.30$ suggests a 30% difference in 2p electron population, most likely in favor of the sp^3 B−H bond. This may help explain the unusual electronic properties of the trispyrazolylborate ligand, in sharing one negative charge, equally, over three symmetry equivalent pyrazolyl nitrogens.

Summary. The present ENDOR studies at Q-band represent, in combination with our previous studies at X-band,[10] the first comprehensive ENDOR study of *any* hs Co(II) system. The data demonstrate that the presence of large unquenched orbital angular momentum in the electronic ground state gives rise to measurably anisotropic Fermi couplings to coordinated ^{14}N. ENDOR of the constitutive ^{1}H is consistent with hyperfine couplings that are dominated by dipolar coupling, with no evidence of π-type interactions through the pyrazole ring system, and analysis of the data supports the presence of significant anisotropy in the relatively small ^{1}H Fermi couplings. The apical ^{11}B show hyperfine couplings also dominated by through-space interactions, with a resolved quadrupole tensor that indicates ~30% electronic asymmetry between the B−H and B−C bonds.

Acknowledgment. The authors wish to thank Byunghoon Lee and Dr. Vladimir M. Grigoryants for assistance with initial ENDOR measurements and Mr. Edwards T. Niles for preparation of the compounds studied. This work was supported by the National Science Foundation (CHE-0518189 and CHE-0809985 to D.L.T.) and the National Institutes of Health (9RO1 EB00326929 and 1 RO1 GM066253-01 to C.P.S.).

Supporting Information Available: Appendix I describes the induction of anisotropy in the Fermi couplings and includes one figure showing the predicted angular behavior of the effective ^{14}N Fermi coupling (Figure S1); Appendix II describes the angular dependence of the anisotropic dipolar couplings and includes four figures that show the predicted angular dependence for the BH proton (Figure S2), the 3H proton (Figure S3), and the 5H proton (Figure S4), as well as a simulations of the experimental 5H proton ENDOR signal near $g_{||}$ (Figure S5) and the field-dependent behavior of the 3H and 5H patterns of Figure 3B (Figure S6) and the field-dependent ^{1}H ENDOR of Co(nBuTp)$_2$ (Figure S7). Also included is one figure showing the relative disposition of ^{1}H and ^{14}N ENDOR features as the applied field is increased (Figure S8). Appendix III outlines the least-squares method utilized in obtaining f_{Co} and A_{iso} and incorporates one figure showing relevant X-band proton ENDOR previously reported in Myers et al.[10] (Figure S9). This material is available free of charge via the Internet at http://pubs.acs.org.

JA900866Y